Heliyon 10 (2024) e33830

Contents lists available at ScienceDirect

Heliyon

journal homepage: www.cell.com/heliyon

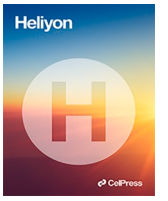

Research article

Rapid multiplex immunohistochemistry for characterizing tumor-immune microenvironment

Alisa Kimura [a], Takahiro Tsujikawa [a,b,*], Hiroki Morimoto [a], Sumiyo Saburi [a], Junichi Mitsuda [a], Shigeyuki Mukudai [a], Hikaru Nagao [a], Saya Shibata [c], Hiroshi Ogi [c,d], Aya Miyagawa-Hayashino [e], Eiichi Konishi [e], Kyoko Itoh [d], Shigeru Hirano [a]

[a] Department of Otolaryngology–Head and Neck Surgery, Kyoto Prefectural University of Medicine, Kyoto, Japan
[b] Department of Cell, Developmental, and Cancer Biology, Oregon Health & Science University, Oregon, USA
[c] SCREEN Holdings Co., Ltd., Kyoto, Japan
[d] Department of Pathology and Applied Neurobiology, Kyoto Prefectural University of Medicine, Kyoto, Japan
[e] Department of Surgical Pathology, Kyoto Prefectural University of Medicine, Kyoto, Japan

A B S T R A C T

Intratumoral immune profiles are related to prognosis and therapeutic efficacy, and could result in personalized treatments based on biomarkers. To develop a multiplex, quantitative, and rapid tissue evaluation method based on the clinically established standard immunohistochemistry (IHC), a 6-marker rapid multiplex IHC was developed based on our previously reported 14-marker multiplex IHC by reducing the number of labels and accelerating the staining procedure. First, fewer labels were required to identify the same immunological features linked to prognosis in 14-marker multiplex IHC analyses. The six selected markers showed a significant correlation with the 14 markers in the immune classification. Next, a rapid staining protocol was developed by optimizing the reaction temperature, chromogen, and washing time, allowing the completion of 6-marker analysis in 5 h and 49 min, as opposed to the several days required for conventional multiplex IHC. Validation of benign tonsil and head and neck cancer tissues revealed a significant correlation between rapid and conventional 6-makrer multiplex IHC in terms of staining intensities, densities of T cells, macrophages, lymphoid/myeloid immune cell ratios, and spatial profiles of intratumoral immune infiltrates. This method may enable quantitative assessment of the tumor-immune microenvironment on a clinically feasible time scale, which promotes the development of tissue biomarker-guided therapeutic strategies.

1. Introduction

The tumor-immune microenvironment (TiME) is intimately involved in the characteristics of solid tumors and is associated with the therapeutic response and resistance to immunotherapy, as well as chemo- and molecular targeting therapies [1]. With the emergence of tissue analytical technologies capable of evaluating the cellular composition, functional states, and spatial organization of TiME components, it has become evident that tissue-based tumor characterization can provide insights into novel targets for therapy, patient stratification, and monitoring of drug response and resistance properties in clinically applicable settings. Currently, various tissue-analyzing technologies, such as single-cell RNA sequencing [2,3] and multiplexed proteomics, are used [4] to examine how cells organize tumors and interact with each other. However, these methods have significant barriers to clinical application in

* Corresponding author. Department of Otolaryngology–Head and Neck Surgery Kyoto Prefectural University of Medicine, 465 Kajiicho, Kamigyoku, Kyoto City, Kyoto, 602-8566, Japan.
E-mail address: tu-ji@koto.kpu-m.ac.jp (T. Tsujikawa).

https://doi.org/10.1016/j.heliyon.2024.e33830
Received 30 December 2023; Received in revised form 28 April 2024; Accepted 27 June 2024
Available online 28 June 2024

terms of time, equipment, and analysis costs. More importantly, the presence of tumor heterogeneity also makes it difficult to elucidate TiME characteristics, as most current advanced methods only analyze a portion of a large tumor section and lack the ability to analyze the entire tissue. The clinical application of biomarkers based on TiME requires the development of techniques that allow rapid analysis of heterogeneous tissue properties with high reliability and cost-effectiveness.

Immunohistochemistry (IHC) is reliably used in pathological diagnosis, allowing pro- and retrospective sample acquisition and tissue-based imaging studies without significant costs; however, classical histological and IHC methods lack multiplex analysis capability. To add multiplicity to standard IHC, multiplex IHC based on iterative cycles of staining, digital image scanning, and antibody/chromogen stripping enables staining with 12–29 different antibodies in a single section, irrespective of the origin of the antibodies [5–7]. Considering the reliability, low cost, and whole-tissue analysis capabilities of standard IHC used in clinical practice, multiplex IHC is advantageous for the quantitative evaluation of multiple cell lineages in a single tissue with preserved spatial information. However, the time-consuming nature of multiplex IHC can be an obstacle to its clinical diagnostic applications. As several endeavors have been made to accelerate conventional multiplex IHC by adjusting the reaction temperature [8,9], electromagnetic fields [10,11], and ultrasound-assisted reactions [12], similar approaches may contribute to the realization of rapid multiplex IHC, which could be adopted in routine clinical practice.

Herein, a rapid multiplex IHC protocol was developed, where our previously reported multiplex IHC protocol with iterative staining cycles [7] was modified to reduce the time required from 2 h to minimum 28 min per cycle. To accelerate multiplex IHC in a short time, the reaction temperatures and washing techniques were optimized, focusing on a minimum of six markers for immune characterization so that the entire process could be completed in less than 6 h. Rapid multiplex IHC has the potential to provide precision medicine based on tissue profiles within a clinically adoptable timeframe.

2. Materials and methods

2.1. Clinical samples and classification

Formalin-fixed paraffin-embedded (FFPE) samples of human tonsils (n = 5) and head and neck squamous cell carcinomas (n = 60) were obtained from surgically resected specimens at the Kyoto Prefectural University of Medicine. Based on a study [7], the classification of the tissue immune characteristics of the three groups of hypo-, lymphoid-, and myeloid-inflamed status was performed as follows: if the number of $CD45^+$ cells was less than 1500 (cells/mm^2), the specimen was classified as hypo-inflamed; otherwise, if the lymphoid-to-myeloid cell ratio was greater than 2, the specimen was classified as lymphoid-inflamed, and if not, the specimen was classified as myeloid-inflamed.

2.2. Multiplex IHC

FFPE tissue sections (5 μm) of FFPE tissues were placed in a 63 °C heat chamber for 15 min, deparaffinized with xylene, and rehydrated in serially graded alcohols in distilled water. Slides were stained with hematoxylin (S3301, Dako) for 2 min, mounted with PBST buffer (x1 D-PBS, Nacalai tesque #14249-66 plus 0.05 % Tween-20), and covered with a cover glass (32 mm No.1, #C024321, or 60 mm No.1, #C024601, Matsunami glass), followed by whole-tissue scanning using a Nanozoomer S60 scanner (Hamamatsu Photonics) at 20× magnification. After removing the cover glass by agitation of the slides in PBST, peroxidase activity was blocked with 0.6 % hydrogen peroxidase in PBS for 15 min, and the slides were subjected to heat-mediated antigen retrieval by immersion in citrate solution (pH 6.0) (LSI Medience, #102172) for 15 min. Sequential multiplex IHC, consisting of iterative cycles of staining, scanning, and antibody/chromogen stripping, was performed.

Conventional multiplex IHC was performed based on the iterative cycles of staining, digital image scanning, and signal stripping as described previously [7]. Briefly, FFPE tumor sections were subjected to protein blocking with a blocking buffer (5.0 % goat serum, 2.5 % BSA, and PBS) for 15 min, followed by sequential immunodetection with primary and horseradish peroxidase (HRP) polymer-conjugated secondary antibodies (Supplementary Table 1). After chromogen development of antibodies based on

Table 1
The list of antibodies and conditions used for rapid multiplex IHC.

	Cycle 1	Cycle 2	Cycle 3	Cycle 4	Cycle 5	Cycle 6
Blocking		1 min	1 min	1 min	1 min	1 min
Primary ab	Hematoxylin	CD68	PDL1	CD45	CD3	pCK
Supplier	Dako	Abcam	Cell Signaling	Thermo Scientific	Thermo Scientific	Abcam
Clone/Product#	S3301	PG-M1	E1L3N	H130	SP7	AE1/AE3
Concentration	Original	1:50	1:100	1:100	1:50	1:2000
Reaction	2 min, room	10 min, 37°C	10 min, 37°C	10 min, 37°C	15 min, 37°C	10 min, 37°C
Secondary ab		Anti-mouse	Anti-rabbit	Anti-mouse	Anti-rabbit	Anti-mouse
Supplier		Nichirei	Nichirei	Nichirei	Nichirei	Nichirei
Product#		414131	414141	414131	414141	414131
Concentration		Original	Original	Original	Original	Original
Reaction		30 min, room	30 min, room	10 min, 37°C	7 min, 37°C	10 min, 37°C
Chromogen		AMEC, 5 min	AMEC, 5 min	AMEC, 5 min	AMEC, 5 min	AMEC, 5 min

3-amino-9-ethylcarbazole (AEC) (Vector Laboratories), the slides were scanned digitally at 20× objective magnification using a Nanozoomer S60 scanner (Hamamatsu Photonics). After chromogenic destaining in an alcohol gradient, tissue sections were stripped of the antibody by heat treatment in a citrate solution (pH 6.0), followed by subsequent rounds of antibody staining and imaging. The conditions and antibodies used for conventional multiplex IHC are listed in a previous report for the 14-plex [13] and Supplementary Table 1 for the 6-plex.

Rapid multiplex IHC was performed using the conventional multiplex IHC method with the following modifications. After protein blocking with blocking buffer (5.0 % goat serum, 2.5 % BSA, and PBS) for 1 min, the sections were incubated with primary antibodies

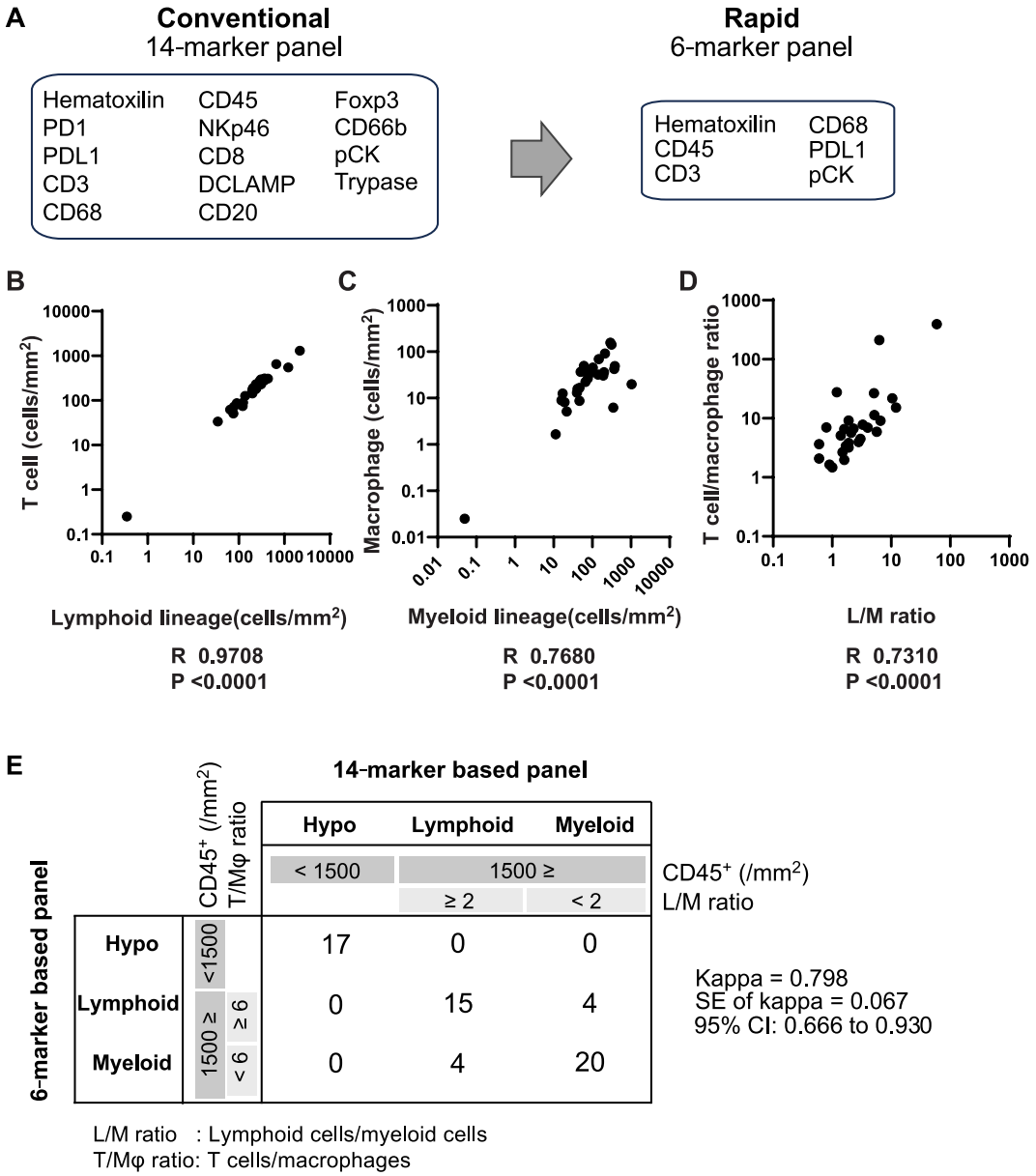

Fig. 1. Six primary immune-related markers represent 14-marker-based tissue immune characteristics. (A) Nuclei, CD68, CD3, PD-L1, CD45, and pan-cytokeratin (pCK) were selected to approximate lymphoid and myeloid cells from the 14-marker panel. (B) Comparative analysis of cell densities between T cells ($CD45^+CD3^+$ cells) in the six-marker panel and lymphoid lineages ($CD45^+CD3^+$ T cells, $CD45^+CD20^+$ B cells, and $CD45^+NKp56^+$ natural killer cells) in the 14-marker panel. (C) Comparative analysis of cell densities between macrophages ($CD45^+CD68^+$ cells) in the six-marker panel and myeloid lineages ($CD45^+CD68^+$ macrophages, $CD45^+CD66b^+$ granulocytes, and $CD45^+Tryptase^+$ mast cells, and $CD45^+DC\text{-}LAMP^+$ dendritic cells) in the 14-marker panel. (D) Correlation between the T cell/macrophage ratio by the 6-marker panel and the lymphoid/myeloid ratio by the 14-marker panel was shown. Statistical assessment (B–D) was performed by Spearman's correlation coefficient. (E) A 3 × 3 contingency table was shown to compare three immunological classifications based on 14-marker versus six-marker panels. Kappa's index was used for statistical assessment.

at the dilutions, reaction times, and temperatures indicated in Table 1. The slides were then stained with either an anti-mouse or anti-rabbit horseradish peroxidase polymer-conjugated antibody (Histofine Simple Stain MAX PO; Nichirei Biosciences Inc.) for the incubation times specified in Table 1. Visualization was performed using an advanced product of AEC, AMEC (Vector Laboratories), which has 5–10 times greater sensitivity than AEC. Cover glass placement, whole-tissue scanning, and cover slip removal were performed as previously described. After chromogenic destaining in an alcohol gradient, the tissue sections were stripped of the antibody by heat treatment in a citrate solution (pH6.0). During each stage, the slides were washed by spraying PBST for approximately 9 s using a squirt bottle. Prior to the chromogen reaction, the slides were washed with deionized water following the PBST wash. The slides were sequentially restored in the order indicated in Table 1. For primary antibodies and HRP polymer-conjugated secondary antibodies, the concentration and reaction time were optimized at 37 °C (Table 1). The reaction temperature was adjusted using an ihcDirect Slide Warmer (#NVD M81500-110, Novodiax).

2.3. Digital image processing and image cytometry

After staining, image acquisition and computational processing were performed as described previously [7]. Iteratively digitized images were accurately co-registered using in-house software (SCREEN Holdings Co., Ltd.). The software calculated the coordinates of each image relative to the reference image (any one of the images). Using these coordinates, a set of non-compressed TIFF images for each region of interest (ROI) was extracted. Visualization was performed using Aperio ImageScope Version 12.March 3, 5048 (Leica) and Image J/Fiji Version 1.51s (National Institutes of Health). Co-registered images were converted to single-marker images; whereafter, they were inverted and converted to grayscale, followed by pseudo-coloring. For quantitative image assessment, single-cell segmentation and quantification of staining intensity and shaped-size measurements were performed using CellProfiler Version 2.2.0 (Broad), and saved in a file format compatible with the image cytometry data analysis software FCS Express 7 Image Cytometry (De Novo Software). The signal intensity of positive cells was determined using thresholds based on the staining intensity of negative controls, as previously described [7].

2.4. Statistical analysis

Statistical calculations were performed using the Spearman's correlation coefficient using GraphPad Prism 8.3.0 (Graphpad

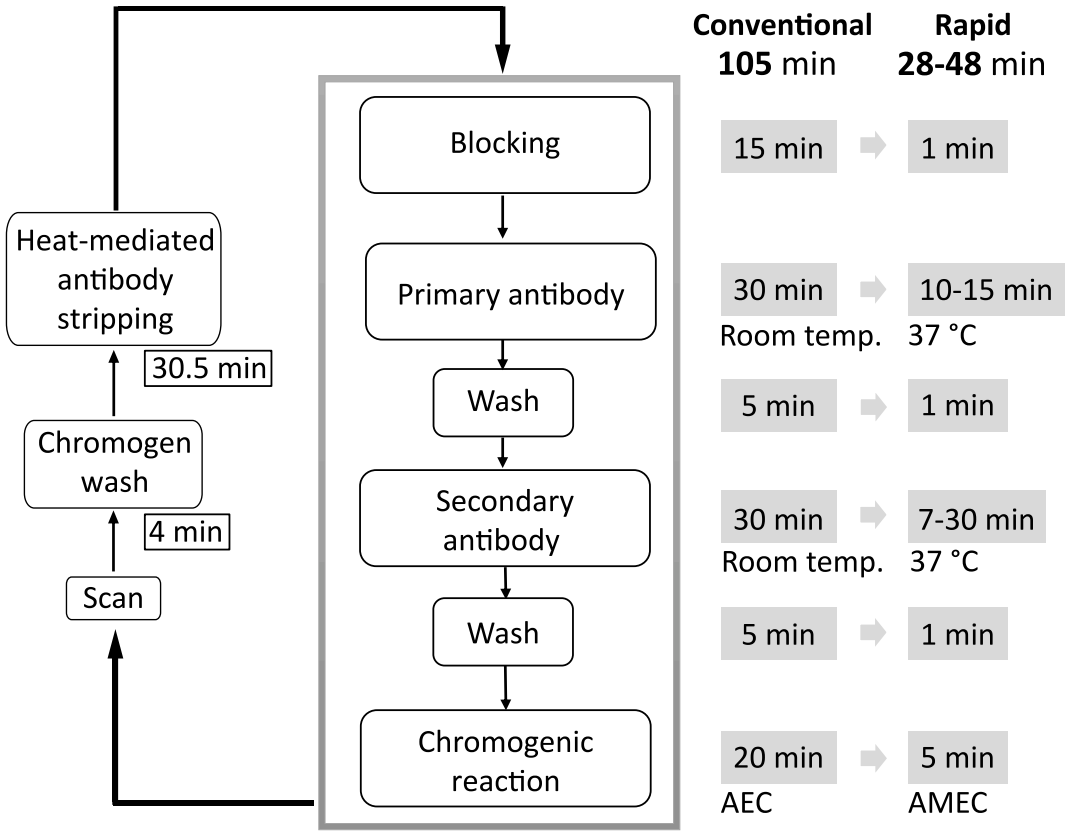

Fig. 2. Rapid multiplex IHC based on enhanced antibody/chromogenic reactions. Schematic overview demonstrates the workflow of the rapid multiplex IHC. Required times for conventional and rapid multiplex IHC are shown (see Materials and methods).

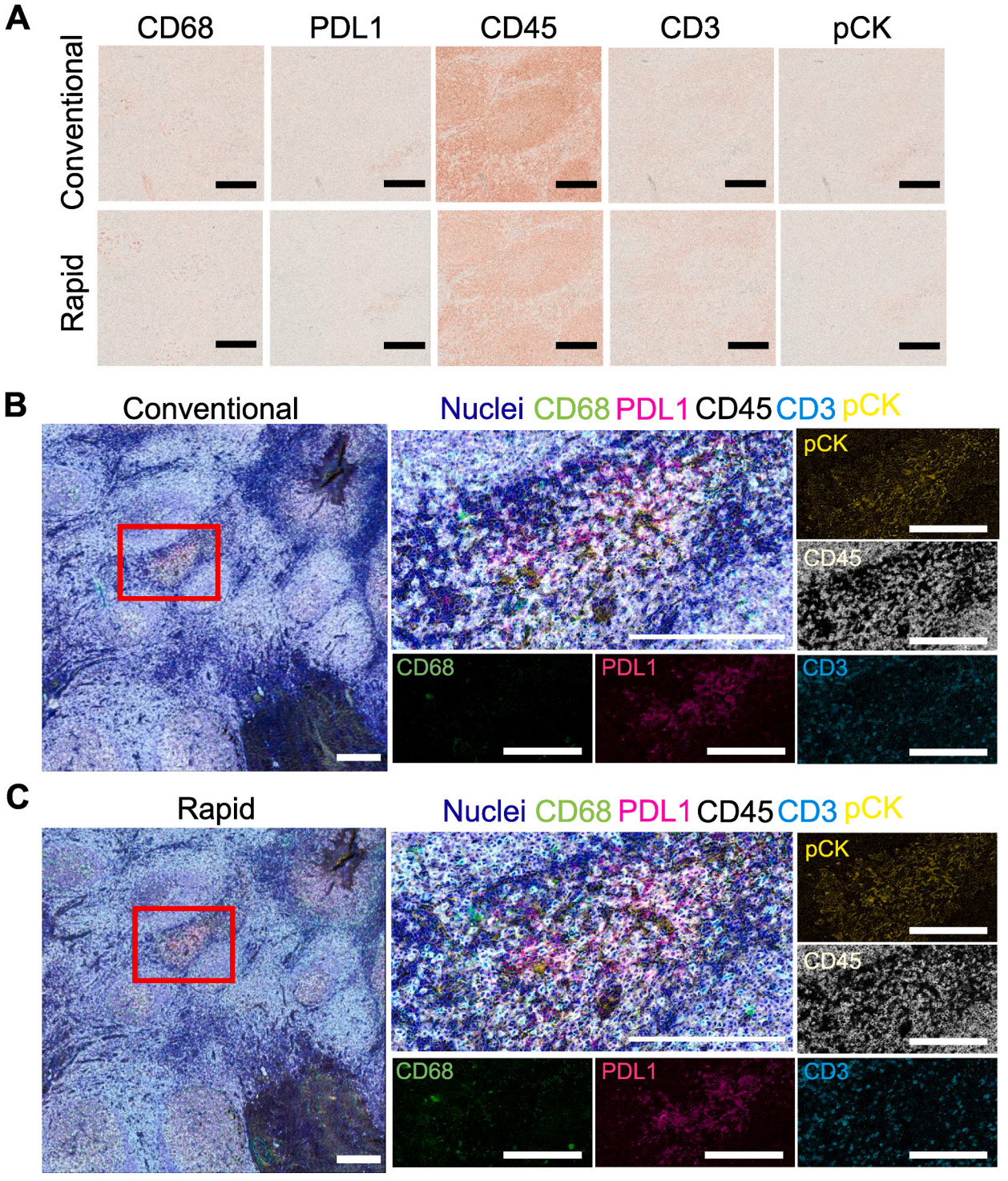

Fig. 3. Rapid and conventional multiplex IHC provide equivalent results in visualization. (A) CD68, programmed cell death ligand 1 (PD-L1), CD45, CD3, and pan-cytokeratin (pCK) were comparatively stained by conventional and rapid protocols in two adjacent serial tissues. Scale bars = 250 μm. (B–C) 6-marker pseudo-colored images stained with conventional (B) and rapid (C) protocols. Biomarkers and colors are shown on top of the images. Corresponding single-marker images are also shown. Scale bars = 250 μm.

Software, San Diego, CA, USA). The kappa index was used to check the agreement of the classification results by conventional and rapid protocols using GraphPad QuickCalc (www.graphpad.com/quickcalcs/kappa1/).

2.5. Study approval

All studies involving human tissues were approved by the Institutional Review Board (ERB-C-43-4) and written informed consent was obtained from all patients.

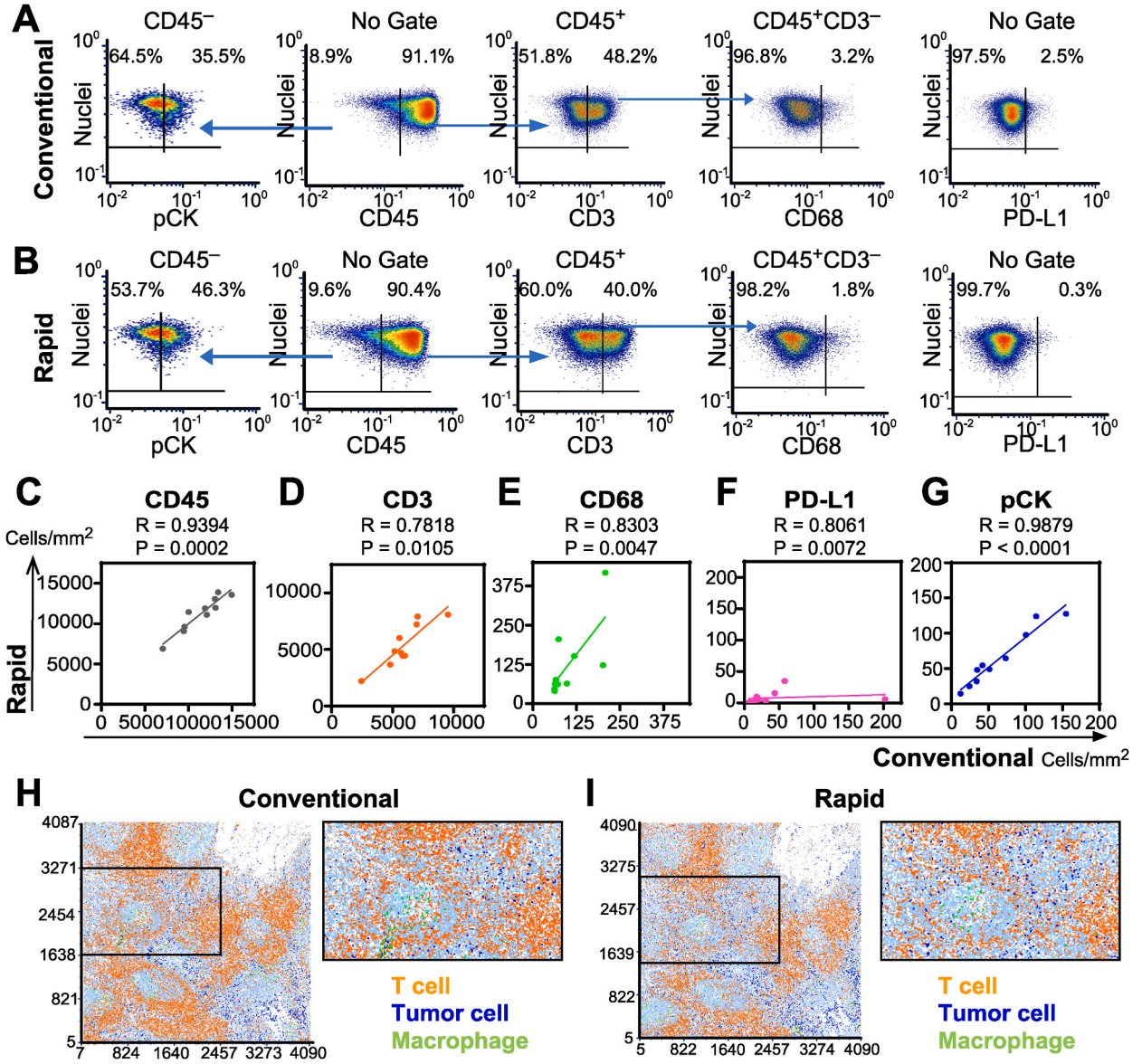

Fig. 4. Multiparameter cytometric image analysis for quantification of multiplex IHC. (A–B) Image cytometry-based cell population analyses for the conventional (A) and rapid procedure (B). Gating thresholds for qualitative identification were determined based on data in negative controls. (C–G) Cell densities quantified by conventional and rapid multiplex IHC compared for CD45 (C), CD3 (D), CD68 (E), programmed cell death ligand 1 (PD-L1) (F), and pan-cytokeratin (pCK) (G), using Spearman's correlation coefficient. (H–I) Location information of single cells on the coordinates, comparing conventional (H) and rapid multiplex IHC (I). The boxes present a magnified region at the right panels. Lineages and color annotations are shown for T cells ($CD45^+CD3^+$), tumor cells (pCK^+), and macrophages ($CD45^+CD68^+$).

3. Results

3.1. Selective six markers represent 14 marker-based immunological characteristics of head and neck squamous cell carcinoma

The balance of lymphoid and myeloid cells, as assessed by 14-marker multiplex staining, is associated with the prognosis of head and neck squamous cell carcinoma, pancreatic ductal adenocarcinoma, and papillary and follicular thyroid carcinomas [7,13]. To achieve rapid staining, the nuclei of CD68, CD3, programmed cell death ligand 1 (PD-L1), CD45, and pan-cytokeratin (pCK) were selected to approximate lymphoid and myeloid cells from the 14-marker panel (Fig. 1A). In the multiplex IHC-based quantitative analysis of 60 specimens of head and neck squamous cell carcinoma, the density of lymphoid and myeloid cells obtained by the 14-marker analysis highly correlated with the density of T cells and macrophages obtained by the 6-marker analysis (Fig. 1B and C).

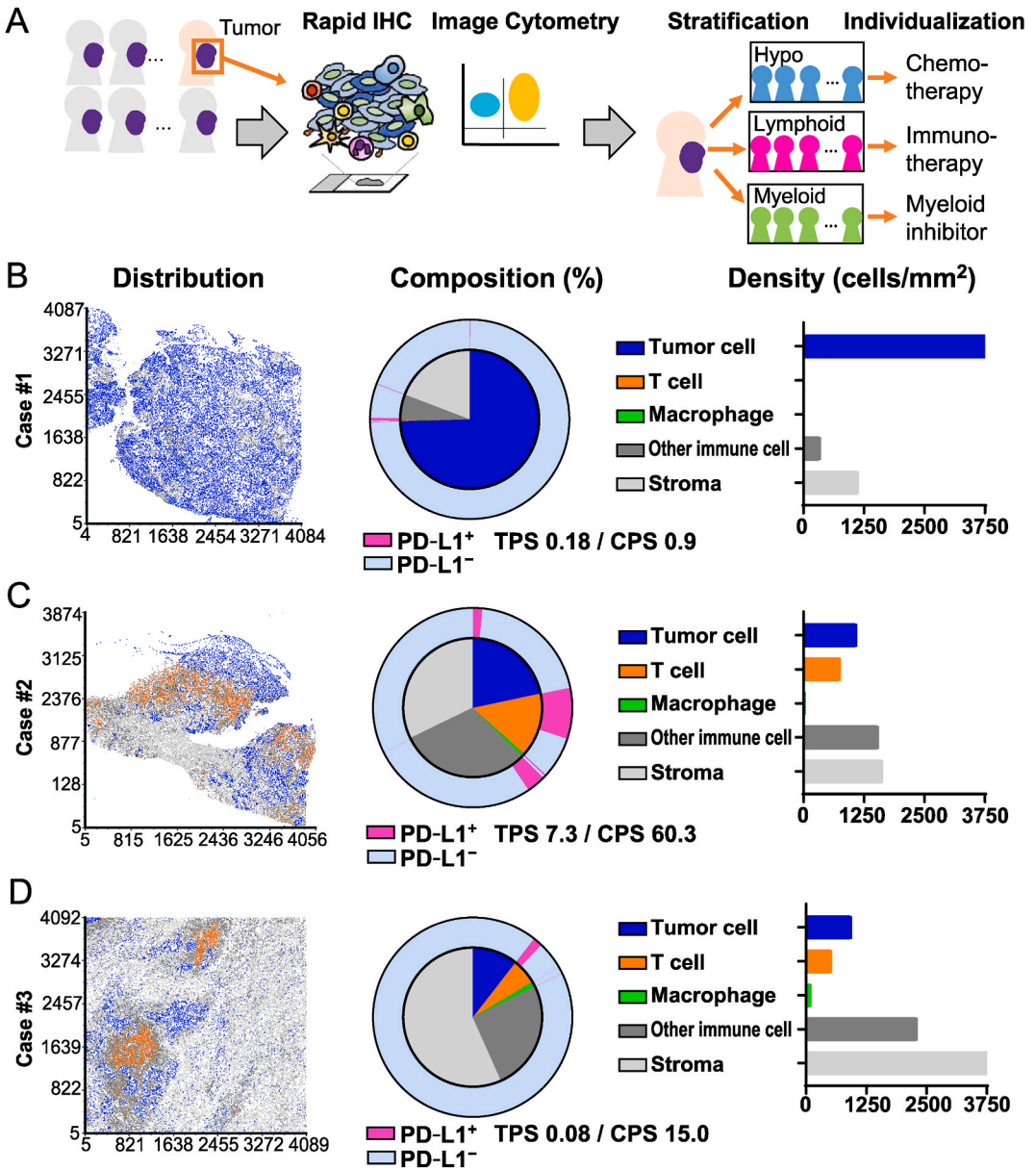

Fig. 5. Demonstration of the rapid multiplex IHC for head and neck squamous cell carcinoma. (A) An overview of rapid multiplex IHC-based biomarker platform. The goal is to select an optimized treatment in a short time by analyzing immunological characteristics. (B–D) Data from three cases analyzed by rapid IHC classified into hypo-inflamed (B), lymphoid-inflamed (C), and myeloid-inflamed (D) profiles. Cell distribution, composition, and density of tumor cells (pCK^+), T cells ($CD45^+CD3^+$), macrophages ($CD45^+CD68^+$), other immune cells ($CD45^+CD3^-CD68^-$), and stroma cells ($CD45^-pCK^-$) are shown. The percentages of PD-$L1^+$ cells are shown in magenta around the perimeter of the pie chart, and tumor proportional score (TPS) and combined positive score (CPS) were calculated.

Furthermore, the lymphoid/myeloid ratio by 14-marker analysis correlated with the T cell/macrophage ratio based on a 6-marker analysis (Fig. 1D). The three subgroups of hypo-, lymphoid-, and myeloid-inflamed profiles based on a previous study (see Materials and methods) were consistent with the classification using the 6-marker panel (Fig. 1E). Together, these results suggest that the six selected markers may enable the prompt estimation of the basic immune properties of tumor tissues.

4. Enhanced antibody/chromogenic reactions enable a rapid procedure of multiplex IHC

Following marker selection, the staining procedure was hastened using two approaches: 1) optimizing the preparatory steps before and after the reaction and 2) enhancing the antigen-antibody reaction (Fig. 2). To optimize the preparatory steps, the protein blocking time was reduced from 15 min to approximately 1 min without affecting the sensitivity and specificity of the antibodies used in this panel. Additionally, reducing the washing time between cycles to 1 min did not compromise sensitivity and specificity. Furthermore, AMEC, instead of AEC, was used for the chromogenic reaction, which has a 5–10 times higher sensitivity and reduced time.

For the enhancement of antigen-antibody reactions, the reaction at 37 °C, which was reported for standard IHC [8], was adopted for our multiplex staining protocol. The reaction time and antibody concentration for the primary and secondary antibodies were optimized for the antigen-antibody reaction at 37 °C (Table 1). The reaction time, which was 30 min at room temperature, was reduced to 10–15 min (Fig. 2 and Table 1). Since 37°C-based secondary antibody reaction for detection of anti-PD-L1 (E1L3N) and anti-CD68 (PG-M1) antibodies did not show improved sensitivities compared with that based at room temperature, the conventional protocol of 30 min at room temperature was adopted (Table 1). These optimizations enabled the entire 6-plex multiplex IHC process to be completed at 5 h and 49 min (Fig. 2).

4.1. Rapid and conventional multiplex IHC provide equivalent results in visualization and quantification

The rapid and conventional methods were compared using adjacent sections of human palatine tonsil tissue. Both methods showed equivalent staining intensities and specificities for CD68, PD-L1, CD45, CD3, and pCK (Fig. 3A–C). To quantitatively validate this result, we extracted 10 ROIs of 2 mm^2 from the whole tissue and compared both methods using image cytometry, which is flow cytometry in images (Fig. 4A and B). Both methods showed significant correlations with CD68, PD-L1, CD45, CD3, and pCK expressions (Fig. 4C–G and Supplementary Fig. 1 A–D). Importantly, T cells, tumor cells, and macrophages identified by both methods exhibited identical distributions (Fig. 4H and I). These findings indicate that the rapid procedure provides equivalent results in terms of visualization and quantification, contributing to the accelerated evaluation of the immunological properties of the tissue.

4.2. Rapid multiplex IHC demonstrates the immunological characteristics of head and neck cancer specimens

Next, we evaluated the TiME using rapid multiplex IHC (Fig. 5A). We applied the rapid protocol to analyze immune-related characteristics of three patients with head and neck squamous cell carcinoma with different clinical outcomes (Fig. 5B–D). An immune-excluded phenotype with low immune cell infiltration was observed in case #1 (Fig. 5B), a high T cell fraction and density was observed in case #2 (Fig. 5C), and a predominant macrophage population was noted for case #3 (Fig. 5D), demonstrating the inter-patient heterogeneity of the TiME, including cellular composition, cell density, and cell distribution. Quantitative single-cell analysis enabled the evaluation of PD-L1 expression as tumor proportional score (TPS) and combined positive score (CPS) (Fig. 5B–D and Supplementary Fig. 2A–C and 3). These results demonstrate that rapid multiplex IHC can rapidly assess the distribution, composition, and density of intratumoral cellular components.

5. Discussion

In this study, a rapid multiplex IHC assay was developed that could assess immune characteristics comparable to a conventional multiplex IHC protocol lasting 6 h. Although numerous studies have demonstrated that TiME characteristics are associated with treatment sensitivity and resistance, there is a gap between research-based discoveries and the development of a clinically applicable biomarker platform in a time- and cost-efficient manner.

The technical advancement in this work is focused on enhancing the antigen–antibody reaction at 37 °C together with optimization of the preparatory steps (Fig. 2). To address potential concerns including tissue damage, degradation, and loss of sensitivity in performing iterative IHC at 37 °C, we have verified that both conventional and rapid multiplex IHC method exhibited comparative visualization and quantification with preserved tissue integrity (Fig. 3). The challenge with this method is that it requires the optimization of appropriate conditions at 37 °C for each antibody; however, this also contributes to the flexibility of customizing the antibody panel according to the purpose and target.

Strategies to individualize treatment based on tumor-immune characteristics have been developed for many types of cancer. As a pioneering example, head and neck cancer can now be staged and treated according to the HPV status or PD-L1 scores by IHC [14,15]. Since it has been theorized that the immunological properties of the tissue are associated with the therapeutic advantages of immunotherapy as well as chemo- and molecular-targeted therapy, it is necessary to develop tissue-based biomarkers in addition to the currently available biomarkers. After a series of procedures over 6 h, our rapid multiplex IHC could serve as a link between academic research and clinical practice, increasing accessibility, and making it feasible to investigate TiME-based biomarkers within a therapeutically reasonable timeframe. The incorporation of biomarkers identified in future TiME studies into a rapid multiplex IHC panel may allow the identification of patients who are likely to benefit from immunotherapy or targeted therapy, including neoadjuvant

therapy and recurrence/metastasis treatment.

The spatial architecture of the immune microenvironment orchestrates tumor immunity and therapeutic responses. Spatial multi-omics analyses revealed the transcriptomes, proteomes, and metabolomes of the TiME in several types of cancers [16–19]. More recently, a seminal study applied deep learning to digital pathology data to explore the interrelations between the TiME and gene mutations in lung cancer [20]. Spatial information has been shown to be related to the clinical prognosis and prediction of TiME, but there is difficulty in TiME research due to the conflict between diversity and whole-tissue analysis. The integration of genetic or transcriptomic information with tissue images provides detailed spatial information; however, the range of analysis is limited. In contrast, multiplex IHC can perform whole tissue analysis and evaluate the spatial relationship of TiME by revealing the distribution of different cellular phenotypes within a single section. The integration of this rapid multiplex IHC platform with various analytical methods currently under development will contribute to a better spatial understanding of cancer tissues and improve accuracy in monitoring and predicting treatment efficacy.

One of the limitations of this study is that the research was performed only on head and neck tissues. Extending this method to other cancer types could broaden its potential applicability in clinical practice. Furthermore, this study was limited to the methodological development, and its utility as a biomarker platform has not yet been validated in the prospective clinical setting. Based on the development of rapid multiplex IHC, predicting therapeutic outcomes, including the effectiveness of immunotherapeutic biomarkers may become feasible by permitting the simultaneous assessment of diagnostic biopsies and the immunological features of cancer tissues, such as the quantity, composition, spatial distribution of immune infiltrates, and clinically applicable PD-L1 scores. This would represent a significant advancement in personalized medicine, allowing for more tailored and effective treatment strategies for patients with malignancies. Taken together, future research should focus on validating this method across various cancer types and in prospective clinical trials to establish its utility as a robust biomarker platform.

In conclusion, a 6-marker rapid multiplex IHC procedure was developed by reducing the number of markers and optimizing the reaction temperature. This method was visually and quantitatively compared and validated with previously established standard techniques and was shown to be capable of analyzing the composition, characteristics, and distribution of immune cells in a short time. Rapid spatial and quantitative assessments of TiME have contributed to the development of novel diagnostic modalities and precision medicine based on tissue profiles.

Ethics statement

This study was reviewed and approved by Institutional Review Board of Kyoto Prefectural University of Medicine, with the approval number: ERB-C-43-4, and written informed consent was obtained from all subjects. All experiments were conducted according to the relevant guidelines and regulations.

Data availability statement

The data supporting the findings of this study are available from the corresponding author upon request.

Sources of support

This study was supported by grants from the Japanese Ministry of Education, Culture, Sports, Science, and Technology (22K09688 and 23K19516); Japan Agency for Medical Research and Development (JP24zf0227002); Public Promoting Association Asano Foundation for Studies on Medicine; and a Research Promotion Award from the Japanese Society of Otorhinolaryngology-Head and Neck Surgery, Inc.

CRediT authorship contribution statement

Alisa Kimura: Writing – original draft, Validation, Methodology, Formal analysis. **Takahiro Tsujikawa:** Writing – review & editing, Methodology, Formal analysis, Conceptualization. **Hiroki Morimoto:** Resources. **Sumiyo Saburi:** Resources. **Junichi Mitsuda:** Resources. **Shigeyuki Mukudai:** Resources. **Hikaru Nagao:** Resources. **Saya Shibata:** Software. **Hiroshi Ogi:** Software. **Aya Miyagawa-Hayashino:** Resources. **Eiichi Konishi:** Resources. **Kyoko Itoh:** Resources. **Shigeru Hirano:** Supervision.

Declaration of competing interest

The authors declare the following financial interests/personal relationships which may be considered as potential competing interests:Takahiro Tsujikawa reports financial support was provided by Japanese Ministry of Education, Culture, Sports, Science, and Technology. Takahiro Tsujikawa reports financial support was provided by Japan Agency for Medical Research and Development. Takahiro Tsujikawa reports financial support was provided by Public Promoting Association Asano Foundation for Studies on Medicine. Takahiro Tsujikawa reports financial support was provided by Research Promotion Award from the Japanese Society of Otorhinolaryngology-Head and Neck Surgery, Inc. Takahiro Tsujikawa reports a relationship with Merck Biopharma that includes: consulting or advisory and speaking and lecture fees. Takahiro Tsujikawa reports a relationship with Merck Sharp & Dohme Corp that includes: speaking and lecture fees. Takahiro Tsujikawa reports a relationship with Eisai Co Ltd that includes: speaking and lecture fees. Takahiro Tsujikawa reports a relationship with Ono Pharmaceutical Co Ltd that includes: speaking and lecture fees. Takahiro

Tsujikawa reports a relationship with Bristol Myers Squibb Co that includes: speaking and lecture fees. Takahiro Tsujikawa reports a relationship with Otsuka Pharmaceutical Factory Inc that includes: speaking and lecture fees. Saya Shibata reports a relationship with Screen Holdings Co Ltd that includes: employment. Hiroshi Ogi reports a relationship with Screen Holdings Co Ltd that includes: employment. Eiichi Konishi reports a relationship with Roche Diagnostics that includes: consulting or advisory. Eiichi Konishi reports a relationship with Chugai Pharmaceutical Co Ltd that includes: speaking and lecture fees. Kyoko Itoh reports a relationship with Screen Holdings Co Ltd that includes: funding grants. If there are other authors, they declare that they have no known competing financial interests or personal relationships that could have appeared to influence the work reported in this paper.

Acknowledgements

The authors thank Ms. Nanako Murakami and Ms. Nana Sakurai for their technical assistance with this project.

Appendix A. Supplementary data

Supplementary data to this article can be found online at https://doi.org/10.1016/j.heliyon.2024.e33830.

References

[1] M. Binnewies, E.W. Roberts, K. Kersten, V. Chan, D.F. Fearon, M. Merad, L.M. Coussens, D.I. Gabrilovich, S. Ostrand-Rosenberg, C.C. Hedrick, R.H. Vonderheide, M.J. Pittet, R.K. Jain, W. Zou, T.K. Howcroft, E.C. Woodhouse, R.A. Weinberg, M.F. Krummel, Understanding the tumor immune microenvironment (TIME) for effective therapy, Nat. Med. 24 (2018) 541–550, https://doi.org/10.1038/s41591-018-0014-x.

[2] Z. Tang, Y. Gu, Z. Shi, L. Min, Z. Zhang, P. Zhou, R. Luo, Y. Wang, Y. Cui, Y. Sun, X. Wang, Multiplex immune profiling reveals the role of serum immune proteomics in predicting response to preoperative chemotherapy of gastric cancer, Cell Rep Med 4 (2023), https://doi.org/10.1016/j.xcrm.2023.100931.

[3] E. Azizi, A.J. Carr, G. Plitas, A.E. Cornish, C. Konopacki, S. Prabhakaran, J. Nainys, K. Wu, V. Kiseliovas, M. Setty, K. Choi, R.M. Fromme, P. Dao, P.T. McKenney, R.C. Wasti, K. Kadaveru, L. Mazutis, A.Y. Rudensky, D. Pe'er, Single-cell map of diverse immune phenotypes in the breast tumor microenvironment, Cell 174 (2018) 1293–1308.e36, https://doi.org/10.1016/j.cell.2018.05.060.

[4] A. Sood, A.M. Miller, E. Brogi, Y. Sui, J. Armenia, E. McDonough, A. Santamaria-Pang, S. Carlin, A. Stamper, C. Campos, Z. Pang, Q. Li, E. Port, T.G. Graeber, N. Schultz, F. Ginty, S.M. Larson, I.K. Mellinghoff, Multiplexed immunofluorescence delineates proteomic cancer cell states associated with metabolism, JCI Insight 1 (2016), https://doi.org/10.1172/jci.insight.87030.

[5] G. Banik, C.B. Betts, S.M. Liudahl, S. Sivagnanam, R. Kawashima, T. Cotechini, W. Larson, J. Goecks, S.I. Pai, D.R. Clayburgh, T. Tsujikawa, L.M. Coussens, High-dimensional multiplexed immunohistochemical characterization of immune contexture in human cancers, Methods Enzymol. 635 (2020) 1–20, https://doi.org/10.1016/BS.MIE.2019.05.039.

[6] S.M. Liudahl, C.B. Betts, S. Sivagnanam, V. Morales-Oyarvide, A. Da Silva, C. Yuan, S. Hwang, A. Grossblatt-Wait, K.R. Leis, W. Larson, M.B. Lavoie, P. Robinson, A.D. Costa, S.A. Väyrynen, T.E. Clancy, D.A. Rubinson, J. Link, D. Keith, W. Horton, M.A. Tempero, R.H. Vonderheide, E.M. Jaffee, B. Sheppard, J. Goecks, R. C. Sears, B.S. Park, M. Mori, J.A. Nowak, B.M. Wolpin, L.M. Coussens, Leukocyte heterogeneity in pancreatic ductal adenocarcinoma: phenotypic and spatial features associated with clinical outcome, Cancer Discov. 11 (2021) 2014–2031, https://doi.org/10.1158/2159-8290.CD-20-0841.

[7] T. Tsujikawa, S. Kumar, R.N. Borkar, V. Azimi, G. Thibault, Y.H. Chang, A. Balter, R. Kawashima, G. Choe, D. Sauer, E. El Rassi, D.R. Clayburgh, M.F. Kulesz-Martin, E.R. Lutz, L. Zheng, E.M. Jaffee, P. Leyshock, A.A. Margolin, M. Mori, J.W. Gray, P.W. Flint, L.M. Coussens, Quantitative multiplex immunohistochemistry reveals myeloid-inflamed tumor-immune complexity associated with poor prognosis, Cell Rep. 19 (2017) 203–217, https://doi.org/10.1016/j.celrep.2017.03.037.

[8] U. Kämmerer, M. Kapp, A.M. Gassel, T. Richter, C. Tank, J. Dietl, P. Ruck, A new rapid immunohistochemical staining technique using the EnVision antibody complex. http://www.jhc.org, 2001.

[9] M. Tsuda, R. Horio, L. Wang, T. Takenami, J. Moriya, J. Suzuka, H. Sugino, Z. Tanei, M. Tanino, S. Tanaka, Novel rapid immunohistochemistry using an alternating current electric field identifies Rac and Cdc 42 activation in human colon cancer FFPE tissues, Sci. Rep. 12 (2022), https://doi.org/10.1038/s41598-022-05892-7.

[10] H. Toda, Y. Minamiya, M. Kagaya, H. Nanjo, Y. Akagami, H. Saito, M. Ito, H. Konno, S. Motoyama, J. Ogawa, A novel immunohistochemical staining method allows ultrarapid detection of lymph node micrometastases while conserving antibody, Acta Histochem. Cytoc. 44 (2011) 133–139, https://doi.org/10.1267/ahc.11006.

[11] M. Tanino, T. Sasajima, H. Nanjo, S. Akesaka, M. Kagaya, T. Kimura, Y. Ishida, M. Oda, M. Takahashi, T. Sugawara, T. Yoshioka, H. Nishihara, Y. Akagami, A. Goto, Y. Minamiya, S. Tanaka, Rapid immunohistochemistry based on alternating current electric field for intraoperative diagnosis of brain tumors, Brain Tumor Pathol. 32 (2015) 12–19, https://doi.org/10.1007/s10014-014-0188-y.

[12] H. Hatta, K. Tsuneyama, T. Kondo, Y. Takano, Development of an ultrasound-emitting device for performing rapid immunostaining procedures, J. Histochem. Cytochem. 58 (2010) 421–428, https://doi.org/10.1369/jhc.2010.955096.

[13] S. Saburi, T. Tsujikawa, A. Miyagawa-Hayashino, J. Mitsuda, K. Yoshimura, A. Kimura, H. Morimoto, G. Ohmura, A. Arai, H. Ogi, E. Konishi, K. Itoh, K. Sugino, S. Hirano, Spatially resolved immune microenvironmental profiling for follicular thyroid carcinoma with minimal capsular invasion, Mod. Pathol. 35 (2022) 721–727, https://doi.org/10.1038/s41379-021-00993-6.

[14] B. Kumar, K.G. Cordell, J.S. Lee, F.P. Worden, M.E. Prince, H.H. Tran, G.T. Wolf, S.G. Urba, D.B. Chepeha, T.N. Teknos, A. Eisbruch, C.I. Tsien, J.M.G. Taylor, N. J. D'Silva, K. Yang, D.M. Kurnit, J.A. Bauer, C.R. Bradford, T.E. Carey, p16 Egfr, H.P.V. titer, Bcl-xL and p53, sex, and smoking as indicators of response to therapy and survival in oropharyngeal cancer, J. Clin. Oncol. 26 (2008) 3128–3137, https://doi.org/10.1200/JCO.2007.12.7662.

[15] J. Gong, A. Chehrazi-Raffle, S. Reddi, R. Salgia, Development of PD-1 and PD-L1 inhibitors as a form of cancer immunotherapy: a comprehensive review of registration trials and future considerations, J Immunother Cancer 6 (2018), https://doi.org/10.1186/s40425-018-0316-z.

[16] E.J. Fertig, E.M. Jaffee, P. Macklin, V. Stearns, C. Wang, Forecasting cancer: from precision to predictive medicine. https://doi.org/10.1016/j.diabres, 2021.

[17] A. Lomakin, J. Svedlund, C. Strell, M. Gataric, A. Shmatko, G. Rukhovich, J.S. Park, Y.S. Ju, S. Dentro, V. Kleshchevnikov, V. Vaskivskyi, T. Li, O.A. Bayraktar, S. Pinder, A.L. Richardson, S. Santagata, P.J. Campbell, H. Russnes, M. Gerstung, M. Nilsson, L.R. Yates, Spatial genomics maps the structure, nature and evolution of cancer clones, Nature 611 (2022) 594–602, https://doi.org/10.1038/s41586-022-05425-2.

[18] J. Ptacek, D. Locke, R. Finck, M.E. Cvijic, Z. Li, J.G. Tarolli, M. Aksoy, Y. Sigal, Y. Zhang, M. Newgren, J. Finn, Multiplexed Ion Beam Imaging (MIBI) for Characterization of the Tumor Microenvironment across Tumor Types, 100, Laboratory Investigation, 2020, pp. 1111–1123, https://doi.org/10.1038/s41374-020-0417-4.

[19] J.M. Wang, R. Hong, E.G. Demicco, J. Tan, R. Lazcano, A.L. Moreira, Y. Li, A. Calinawan, N. Razavian, T. Schraink, M.A. Gillette, G.S. Omenn, E. An, H. Rodriguez, A. Tsirigos, K.V. Ruggles, L. Ding, A.I. Robles, D.R. Mani, K.D. Rodland, A.J. Lazar, W. Liu, D. Fenyö, F. Aguet, Y. Akiyama, S. Anand, M. Anurag, Ö. Babur, J. Bavarva, C. Birger, M.J. Birrer, L.C. Cantley, S. Cao, S.A. Carr, M. Ceccarelli, D.W. Chan, A.M. Chinnaiyan, H. Cho, S. Chowdhury, M.P. Cieslik, K. R. Clauser, A. Colaprico, D.C. Zhou, F. da Veiga Leprevost, C. Day, S.M. Dhanasekaran, M.J. Domagalski, Y. Dou, B.J. Druker, N. Edwards, M.J. Ellis, M. E. Selvan, S.M. Foltz, A. Francis, Y. Geffen, G. Getz, T.J. Gonzalez Robles, S.J.C. Gosline, Z.H. Gümüş, D.I. Heiman, T. Hiltke, G. Hostetter, Y. Hu, C. Huang, E. Huntsman, A. Iavarone, E.J. Jaehnig, S.D. Jewell, J. Ji, W. Jiang, J.L. Johnson, L. Katsnelson, K.A. Ketchum, I. Kolodziejczak, K. Krug, C. Kumar-Sinha, J. T. Lei, W.-W. Liang, Y. Liao, C.M. Lindgren, T. Liu, W. Ma, F.M. Rodrigues, W. McKerrow, M. Mesri, A.I. Nesvizhskii, C.J. Newton, R. Oldroyd, A.G. Paulovich, S. H. Payne, F. Petralia, P. Pugliese, B. Reva, D. Rykunov, S. Satpathy, S.R. Savage, E.E. Schadt, M. Schnaubelt, S. Schürer, Z. Shi, R.D. Smith, X. Song, Y. Song, V. Stathias, E.P. Storrs, N.V. Terekhanova, R.R. Thangudu, M. Thiagarajan, N. Tignor, L.-B. Wang, P. Wang, Y. Wang, B. Wen, M. Wiznerowicz, Y. Wu, M. A. Wyczalkowski, L. Yao, T.M. Yaron, X. Yi, B. Zhang, H. Zhang, Q. Zhang, X. Zhang, Z. Zhang, Deep learning integrates histopathology and proteogenomics at a pan-cancer level, Cell Rep Med 4 (2023) 101173, https://doi.org/10.1016/j.xcrm.2023.101173.

[20] S. Wang, R. Rong, D.M. Yang, J. Fujimoto, S. Yan, L. Cai, L. Yang, D. Luo, C. Behrens, E.R. Parra, B. Yao, L. Xu, T. Wang, X. Zhan, I.I. Wistuba, J. Minna, Y. Xie, G. Xiao, Computational staining of pathology images to study the tumor microenvironment in lung cancer, Cancer Res. 80 (2020) 2056–2066, https://doi.org/10.1158/0008-5472.CAN-19-1629.